Oxygen Reduction on Carbon-Supported Pt−Ni and Pt−Co Alloy Catalysts

U. A. Paulus,* A. Wokaun, and G. G. Scherer

Paul Scherrer Institut, Laboratory for Electrochemistry, CH-5232 Villigen PSI, Switzerland

T. J. Schmidt, V. Stamenkovic, V. Radmilovic, N. M. Markovic, and P. N. Ross

Materials Sciences Division, Lawrence Berkeley National Laboratory, University of California, Berkeley, California 94720

Received: September 10, 2001; In Final Form: January 23, 2002

We describe a comparative study of the oxygen reduction reaction on two carbon-supported Pt-based alloy catalysts in aqueous acidic electrolyte at low temperature. Both alloys have the bulk compositions of 50 and 75 at. % Pt, with the alloying elements being Ni and Co. Comparison is made to a pure Pt catalyst on the same carbon support, Vulcan XC-72, having the same metal loading (20 wt %) and nominally the same particle size (4 ± 2 nm). High-resolution electron microscopy was used to determine the size and shape of the particles as well as the particle size distribution on all catalysts. Electrochemical measurements were performed using the thin-film rotating ring−disk electrode method in 0.1 M $HClO_4$ at 20−60 °C. Hydrogen adsorption pseudocapacitance was used to determine the number of Pt surface atoms and to estimate the surface composition of the alloy catalysts. Kinetic analysis in comparison to pure Pt revealed a small activity enhancement (per Pt surface atom) of ca. 1.5 for the 25 at. % Ni and Co catalysts, and a more significant enhancement of a factor of 2−3 for the 50 at. % Co. The 50 at. % Ni catalyst was less active than the Pt standard and unstable at oxygen electrode potentials. Ring-current collection measurements for peroxide indicated no significant differences between the Pt−Co catalysts or the 25 at. % Ni catalyst and pure Pt, while the 50 at. % Ni catalyst had a higher peroxide yield. Together with the observed Tafel slopes and activation energies, it was concluded that the kinetic enhancement is contained in the preexponential factor of the conventional transition state theory rate expression. It is, however, not clear why the alloying with Ni or Co produces this change in the preexponential factor.

1. Introduction

The understanding of the kinetic limitations of the oxygen reduction reaction (ORR) on different catalysts is a problem of outstanding interest in fuel cell research. Carbon-supported platinum catalysts still serve as the most widely used electrocatalyst in the air electrode in low-temperature polymer electrolyte fuel cells (PEFCs).[1] Kinetic limitations for the ORR lead to cell voltage losses (versus the theoretical potential) of at least 0.3 to 0.4 V under typical PEFC operating conditions.[1] Ineffective electrode structures increase the voltage losses even further. However, intensive engineering of the membrane electrode assembly has removed most of those losses, resulting in the use of extremely thin catalyst layers with Pt loading as low as 0.12 mg/cm^2.[2,3] Further improvements in PEFC cell voltage will require finding a catalyst more active than Pt for the ORR. A variety of binary and ternary Pt-alloy systems have been discussed and investigated during the last twenty years for use in either phosphoric acid fuel cells (PAFC) or polymer electrolyte fuel cells (PEFC). An overview with emphasis on the patent literature was presented by Stonehart.[4] The results are contradictory. For example, Luczak et al.[5−7] claimed an increase of a factor of 1.5 to 2.5 in mass activity (mA/mg Pt at 0.9 V) using Pt−Co−Cr or Pt−Cr "alloy" catalysts instead of pure Pt in PAFCs. On the other hand, Beard and Ross[8] and Glass et al.[9] did not find an increased mass activity for Pt−Co or Pt−Cr (75% Pt) in comparison to pure Pt. Both the latter studies also reported that the transition metal was lost from the alloy during testing as an oxygen electrode in a PAFC. More recent half-cell experiments in 190 °C phosphoric acid reported enhancement factors of 2 to 5 when using Pt−Cr, Pt−Co or Pt−Ni versus pure Pt.[10] In the case of testing in PEFCs, Mukerjee et al.[11−13] and Tamizhmani et al.[14] found a similar activity enhancement (factors of 2−3) when using Pt−Co, Pt−Ni or Pt−Cr versus Pt. Toda et al.[15] reported enhancement factors of as much as 10 for sputtered films of Pt−Ni, Pt−Co and Pt−Fe in comparison to a similarly prepared pure Pt film in 0.1 M $HClO_4$ at room temperature. On the other hand, ORR measurements in this laboratory with well-characterized Pt−Ni and Pt−Co bulk alloy electrodes in aqueous acidic electrolyte at PEFC conditions again found much smaller enhancements (factors of 1.5−2) versus similarly well-characterized polycrystalline Pt.[16]

With the exception of the results by Toda et al.[15] all of the reports of enhancement with transition metal alloying to Pt have been reported using carbon-supported catalysts. Studies using well-characterized bulk alloys with nominally the same composition failed to observe this enhancement. As pointed out previously by Beard and Ross,[8] the comparison between alloy catalysts and pure Pt must be done carefully, recognizing that the activity of the Pt and/or the alloy may depend on particle size, and regardless of the normalization procedure one should compare results at or near the same particle size. That was

* Corresponding author: Phone: (41) 56 310 20 59. Fax: (41) 56 310 44 15. E-mail: ursula.paulus@psi.ch.

10.1021/jp013442l CCC: $22.00 © 2002 American Chemical Society
Published on Web 03/29/2002

generally not the case in the previous studies cited above. We report here the results from a study of two different carbon-supported alloy catalysts in comparison to pure Pt on the same support with the same metal loading (20 wt %) and close to the same particle size, 4 ± 2 nm. High-resolution transmission electron microscopy (HRTEM) analysis provided information about the particle size and shape. Quantitative kinetic measurements for the ORR were made using the thin-film rotating ring−disk electrode (RRDE) method.[17] This technique allows the accurate determination of kinetic data such as Tafel slopes, reaction orders and (apparent) activation enthalpies in the absence of mass transport effects. Ring current measurements provide the parallel determination of the product distribution (H_2O_2 versus H_2O formation) under PEFC relevant conditions[18,19] and give insight to the reaction pathway. Finally, we compare our results of these supported alloys to results obtained with carefully prepared smooth polycrystalline bulk alloys of the same stoichiometry.[16]

2. Experimental Section

We used commercially available Pt-based fuel cell catalysts provided by E-TEK (Natick, MA), 20 wt % Pt supported on Vulcan XC72 carbon black, and two alloy catalysts, also 20 wt % metal on Vulcan XC72 (Cabot) carbon black with overall stoichiometries of 50 at. % Ni (Co) and 25 at. % Ni (Co). The catalysts were all used as-received. X-ray diffraction analysis of the four alloy catalysts using a conventional powder diffractometer (Siemens D-500) revealed only a single fcc phase in each, with lattice constants of 0.365 nm (25 at. % Ni) and 0.375 nm (50 at. % Ni) for the Pt−Ni, and 0.384 nm (25 at. % Co) and 0.374 nm (50 at. % Co) for the Pt−Co catalyst. These values are in reasonable agreement with the lattice constants for the corresponding bulk solid solutions.[20] Hereafter, we shall refer to these two alloy catalysts as Pt_3Ni (Co) and PtNi (Co), respectively, although it should be understood that these are solid solutions and *not* ordered phases (or intermetallic compounds). Pt−Co does form ordered phases at 25 and 50 at. % compositions, and the ordered phase Pt_3Co was reported by Beard and Ross[8] in their carbon-supported Pt−Co catalyst heat-treated at relatively high temperatures (e.g., >900 °C).

2.1. High-Resolution Electron Microscopy (HREM). Specimens were prepared for transmission electron microscopy by making suspensions of the catalyst powders in ethanol, using an ultrasonic bath. These suspensions were dropped onto clean holey carbon grids, which were then dried in air. Samples were examined using the OO2B and ARM high-resolution electron microscopes at the National Center for Electron Microscopy (NCEM), Berkeley. The particle shapes were determined by real-space crystallography using high-resolution images taken from particles near or on the edge of the carbon black substrate. Structural information on single particles was obtained by numerical Fourier filtering of the digitized image intensity spectrum. Dark-field imaging was also utilized in order to investigate the overall distribution of metallic particles on the carbon black.

2.2. Electrode Preparation and Electrochemical Measurements. Electrochemical measurements were conducted in a thermostated standard three-compartment electrochemical cell with reference and counter electrodes in separate compartments from the working electrode. The working electrode is a commercial (Pine Instruments) ring−disk electrode with an insertable (interchangeable) disk, in this case glassy carbon covered by a thin layer of catalyst imbedded in a recast Nafion polymer electrolyte film. Ring and disk potential were controlled with a bi-potentiostat (Pine Instruments). For the collection experiments, the Pt ring electrode was potentiostated at 1.2 V versus the reversible hydrogen electrode (RHE) where the detection of peroxide is diffusion limited. The collection efficiency, N, for these thin-films electrodes was determined to be 0.2.[21] The reference electrode is a saturated calomel electrode (SCE), separated from the working electrode compartment by a closed electrolyte bridge in order to avoid chloride contamination. The potentials in this study, however, all refer to that of the RHE.

The thin catalyst layers were prepared as described in our preceding publications.[17,18] In short, glassy carbon disk electrodes (Sigradur G, Hochtemperatur Werkstoffe GmbH, 6 mm diameter) polished to a mirror-finish prior to each experiment (0.1 μm alumina, Buehler) served as substrates for the supported catalysts. In each case 20 μL of ultrasonically re-dispersed catalyst suspension (1.0 $mg_{catalyst}$/mL) in triply pyrodistilled water was pipetted onto the glassy carbon substrate, resulting in a constant metal loading of 14 $\mu g_{metal}/cm^2$. After drying in flowing high-purity argon at room temperature, the deposited catalyst was then covered with 20 μL of a diluted aqueous Nafion solution prepared similarly to the method described by Denton et al.[22] After drying, the final thickness of the layer, measured with a profilometer, was typically ~0.2 μm. After preparation, electrodes were immersed under potential control (at 150 mV) in argon-purged electrolyte (Bay Gas Research Purity). For the oxygen reduction experiments, the electrolyte was saturated with oxygen (Bay Gas Research Purity) bubbled through the electrolyte. The electrolyte itself, 0.1 M $HClO_4$, was prepared from 70% $HClO_4$ (Baker Ultrex) with triply pyrodistilled water.

3. Results and Discussion

3.1. Catalyst Characterization. The carbon-supported catalysts were characterized by HREM. Figures 1−5 present the HREM analysis of Pt, Pt_3Ni, PtNi, Pt_3Co, and PtCo, respectively. Low-magnification images (part A) illustrate that the distribution of the metal particles on the carbon support is uniform and in a narrow particle size range. The histograms of the particle size distribution (part B), which include analyses of several different regions, reflect quantitatively the uniform distribution with an average mean particle size of 3 to 4 nm for all catalysts. It is evident that the particle size distribution is slightly broader in case of the alloy catalysts with an enhanced fraction of particles larger than 5 nm. The mean particle diameter, d, was calculated according to eq 1, and the surface averaged dispersion, D (ratio of atoms in the particles that are on the surface to the total number of atoms in the particles), was calculated from eq 2,

$$d = \frac{\sum_i n_i d_i}{n_i} \tag{1}$$

$$D = 6\frac{v}{s}\frac{\sum_i n_i d_i^2}{\sum_i n_i d_i^3} \tag{2}$$

where n_i is the frequency of occurrence of particles of the size d_i, v is the volume per metal atom in the bulk, and s is the average area occupied by a metal atom in the surface. The prefactor 6 is valid for spherical particles. For determining the

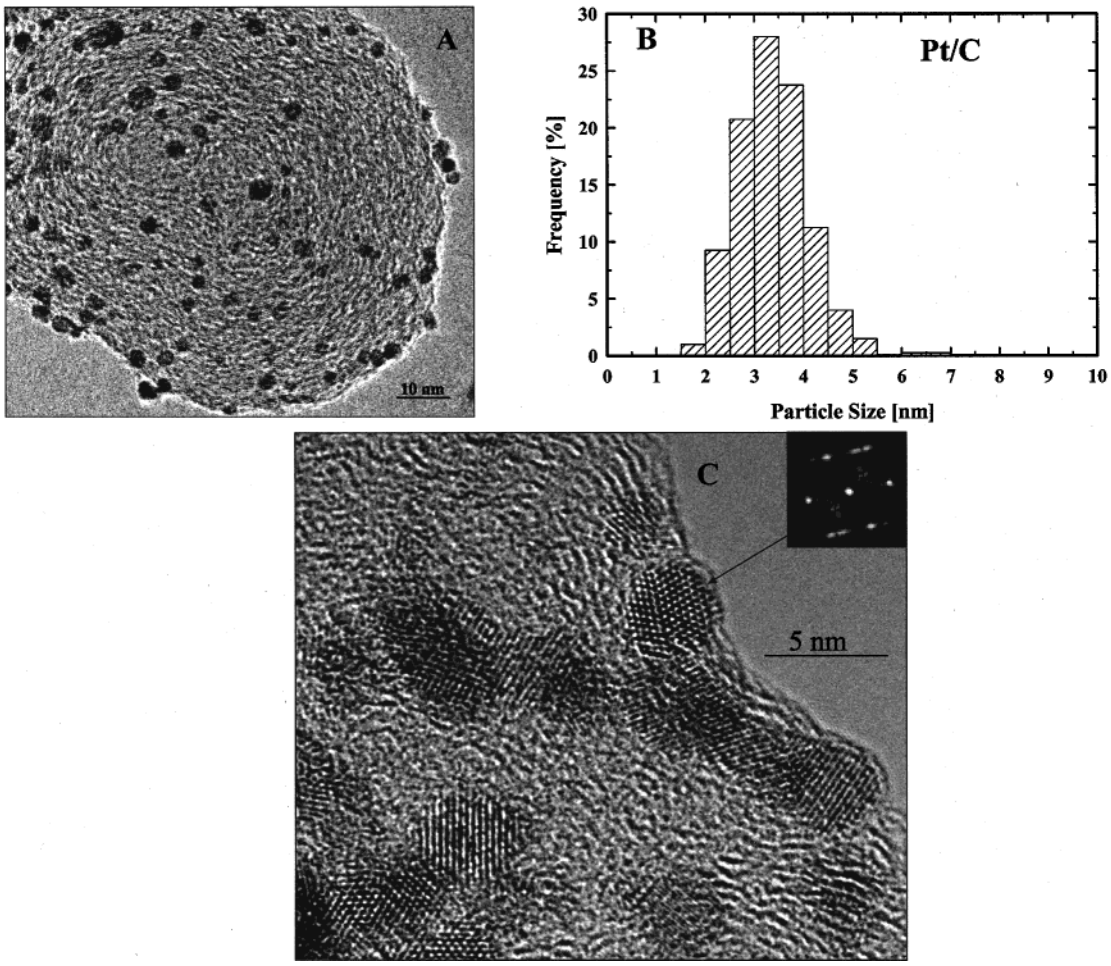

Figure 1. (a) Low-magnification HREM micrograph. (b) Particle size distribution determined by HREM micrographs. (c) HREM micrograph with atomic resolution of the standard supported Pt catalyst.

TABLE 1: Comparison of Physical Properties of the Different Investigated Catalysts

catalyst	mean particle diameter *d* (nm)	dispersion *D* (%)
Pt/Vulcan	3.4 ± 1.2	30
PtNi/Vulcan	4.1 ± 1.2	23
Pt_3Ni/Vulcan	4.0 ± 0.9	25
PtCo/Vulcan	4.4 ± 2.6	19
Pt_3Co/Vulcan	3.4 ± 0.7	29

particle size distribution from low-magnification images, all particles were considered to be spherical, but in fact, the most frequent particle shape is cubooctahedral. These resulting values of *d* and *D* are summarized in Table 1. According to these data, the alloy particles are roughly 20% larger than the pure platinum particles. Table 2 summarizes several other measures of the distribution of metal atoms in the catalysts. The first (column 1) is the metal atom density per geometric electrode area. Due to the substitution of Pt by the smaller and lighter Ni (Co) atoms, equal metal loading means higher densities of metal atoms per geometric area using the alloy catalysts. The surface atomic density (column two) is calculated using the atomic density per geometric area of the electrode and the dispersion and is the number of surface metal atoms per unit area of electrode. If the surface composition of the metallic particle is known, then the absolute number of Pt surface atoms per unit area electrode can be obtained, as shown in column 4 of Table 2. This is discussed further in the next section.

Elemental distributions were also obtained using X-ray emission spectroscopy. A Ni(Co) map image at low magnification (as in part A) obtained via the X-ray emission energy filtering imaging technique (data not shown) indicated that every particle contains both Pt and Ni(Co) atoms. Thus, we can exclude the presence of unalloyed domains of Pt or Ni(Co) nanoclusters on the supported catalysts. Quantitative analysis performed on several particles revealed compositions of 75 ± 5% platinum for the Pt_3Ni(Co) catalyst and 50 ± 5% platinum for the PtNi(Co) catalyst, respectively. This was a reasonable, but not definitive, indication that all metallic particles have the same composition as the bulk stoichiometry, i.e., Pt:Ni(Co) = 3:1 and 1:1.

TABLE 2: Comparison of Theoretical Atomic Densities and the Experimentally Determined Active Surface Area

catalyst	metal atom density (nmol/cm^2)	metal atom surface density (nmol/cm^2)	charge H_{upd}-region (mC/cm^2)	active (Pt) surface atoms (nmol/cm^2)	estimated surface composition (%)
Pt/Vulcan	72.4	21.7	1.97	20.4	(100)
PtNi/Vulcan	111.4	25.6	0.5	5.0	20
Pt_3Ni/Vulcan	87.8	22.0	1.5	15.8	70
PtCo/Vulcan	111.4	21.2	0.72	7.5	35
Pt_3Co/Vulcan	87.8	25.2	1.4	14.5	58

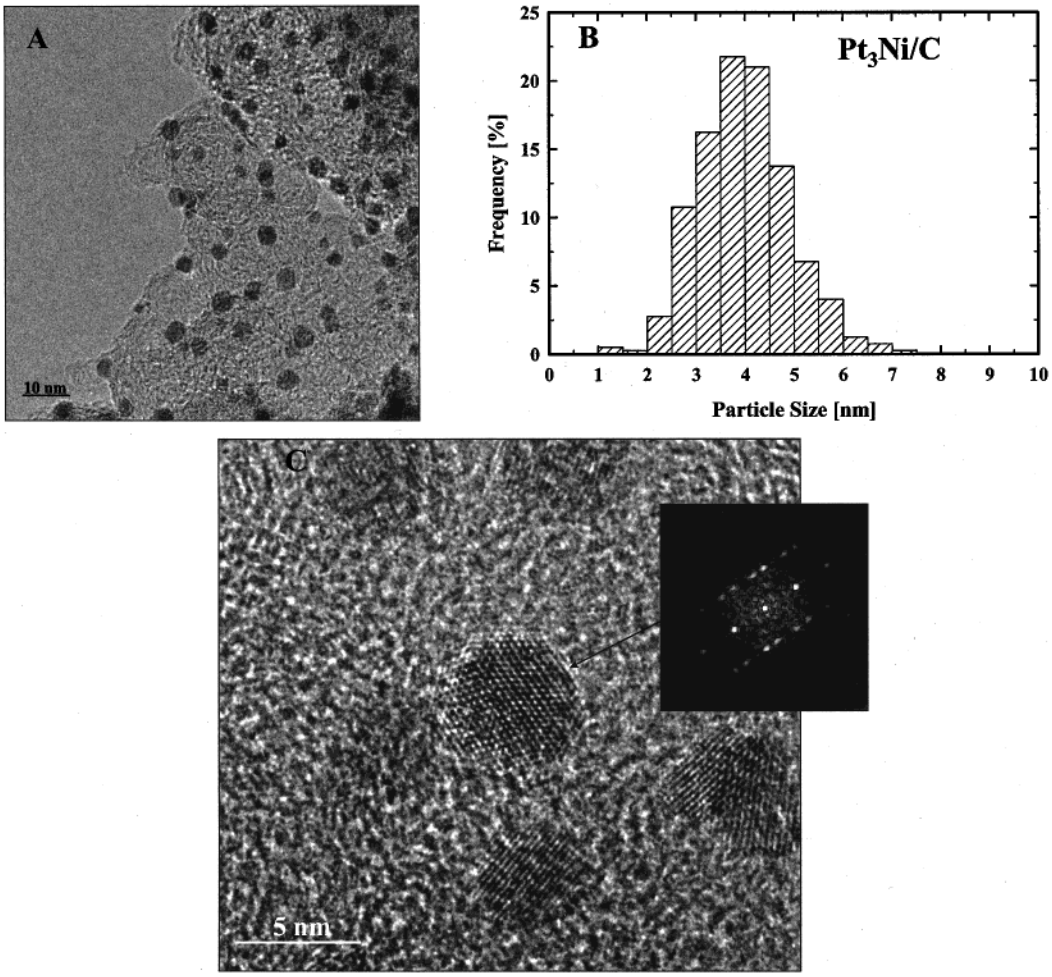

Figure 2. (a) Low-magnification HREM micrograph. (b) Particle size distribution determined by HREM micrographs. (c) HREM micrograph with atomic resolution of the Pt-25 at. % Ni (Pt_3Ni) catalyst.

Finally part C of Figures 1−5 show a high-magnification HREM micrograph along with a microdiffraction pattern from a single particle in each of the three catalysts. Some twinned particles were observed in all five catalysts, even in the pure Pt. The Pt−Ni catalysts had the highest number of twinned particles, but in all cases twinned particles were relatively rare. The most frequent structure of a typical Pt particle shows a cubooctahedral form, while the two alloy catalysts, however, both revealed a more spherical form.

3.2. Electrochemical Measurement. *3.2.1. Cyclic Voltammetry*. The catalysts were first characterized electrochemically by cyclic voltammetry. Therefore electrodes were cycled several times between 0 and 0.9 V at room temperature in an argon purged electrolyte. The resulting voltammograms are presented in Figure 6 for the supported Pt, PtNi and Pt_3Ni catalysts, and in Figure 7 for the Pt, PtCo, and Pt_3Co catalysts. Except for the PtNi catalyst, no changes in the voltammograms were observed during this initial cycling procedure. Aside from this difference, the base voltammetry of the Ni and Co catalysts are essentially identical, and in the following the features are discussed as related to both. The area in the hydrogen underpotential deposition (H_{upd}) region, i.e., the adsorption pseudocapacitance, decreases with decreasing Pt-content. The shape of the H_{upd} region of the 75% Pt catalyst is very similar to that of the Pt catalyst and shows the same typical H-adsorption and desorption features in the potential region between 50 and 300 mV. However, the H_{upd} region of the 50% Pt catalyst is nearly featureless, and none of the H_{upd} peaks typical for polycrystalline platinum are resolved.

To determine the electrochemically active surface area, the H_{upd} region of the different base voltammograms was integrated applying the procedure described in ref 17. The obtained H_{upd} charges are listed in Table 2 (column 3). It is known that in case of pure Pt, the number of surface atoms can be obtained from the charge in the H_{upd} region.[23] The calculated number of electrochemically active surface atoms is in excellent agreement with the value calculated from electron microscopy, i.e., the particle size distribution. If we assume that alloying with Ni(Co) does not effect the binding of H_{upd} to the Pt surface atoms, we can again estimate the number of platinum surface atoms present on the alloy particles from the determined H_{upd} charge (note that this method was proven to be well suitable on UHV prepared well-defined Pt_3M bulk electrodes[24]). The number of active surface atoms obtained thereby (column 4) allows the estimation of the particle surface composition (column 5). For the $Pt_3Ni(Co)$ catalyst, we find 70% Pt on the surface of the Pt_3Ni particles and 58% Pt on the surface of the Pt_3Co particles. The value for Pt_3Ni is very close to the bulk composition of 75 at. % Pt and indicates that no segregation has taken place, whereas in case of the Pt_3Co a slight surface segregation of Co is observed. For the PtNi catalyst, however, we find only about 20 at. % surface Pt and for the PtCo catalyst 35% surface Pt, indicating Ni(Co) segregation to the surface. However, unlike the PtCo catalyst, the base voltammetry of PtNi changes substantially over the whole period of measurement

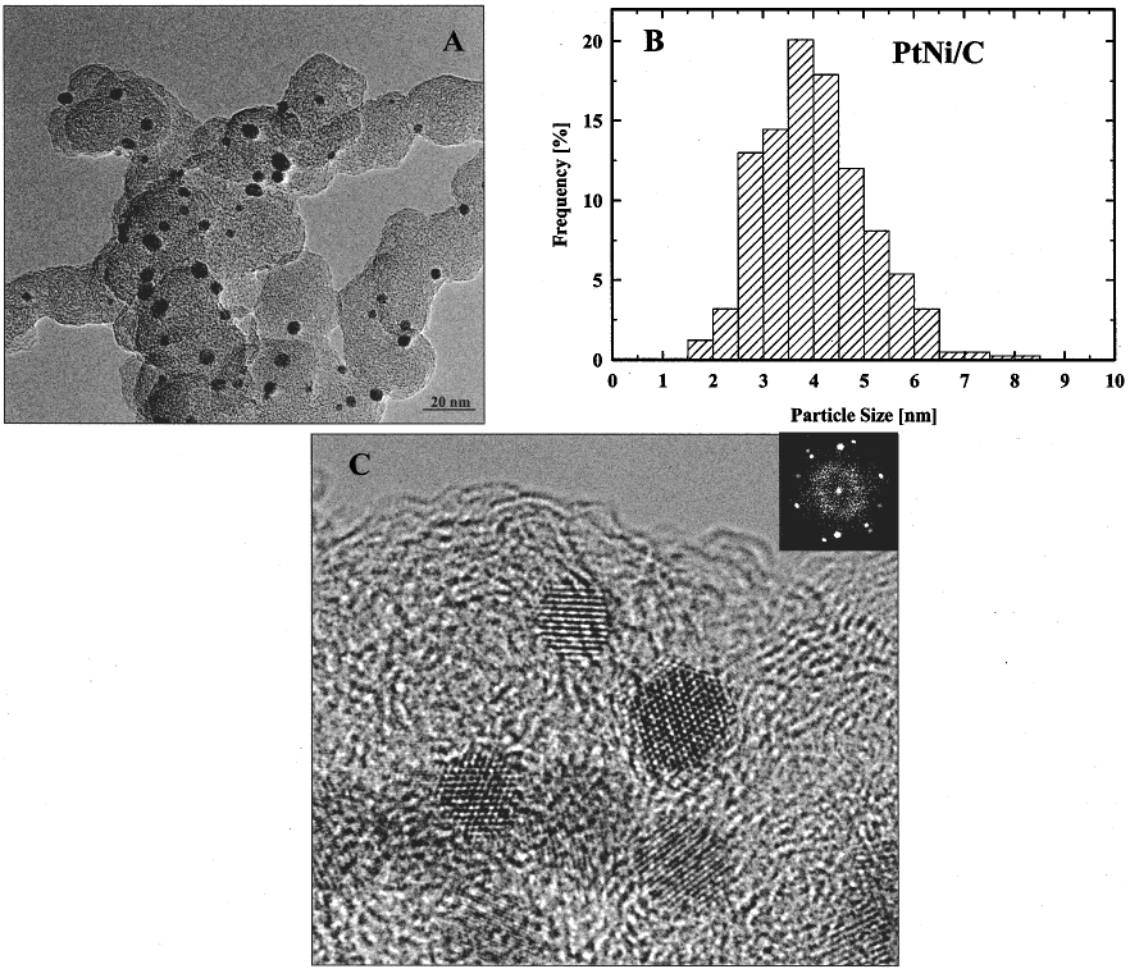

Figure 3. (a) Low-magnification HREM micrograph. (b) Particle size distribution determined by HREM micrographs. (c) HREM micrograph with atomic resolution of the Pt-50 at. % Ni (PtNi) catalyst.

(including the measurement of ORR kinetics), particularly after measurements above room temperature. The nature of these changes is that the base voltammetry becomes more "Pt-like", probably indicative of leaching of Ni from the surface. The instability of the PtNi catalyst in the ORR environment makes interpretation of the results with this catalyst problematic.

Finally, from the base voltammetry we note that the onset of oxide formation shifts to more positive potentials with increasing Ni or Co content. For pure Pt, oxide formation in the anodic going sweep starts at around 700 mV, whereas on $Pt_3Ni(Co)$ the onset can be observed at around 750 mV, and on PtNi(Co) between 750 and 800 mV. This may indicate that alloying with Ni(Co) effects a fundamental change in the way Pt atoms interact with H_2O and possibly O_2, and this change could be manifested in the kinetic measurements.

3.2.2. Oxygen Reduction Reaction (ORR) Kinetics. Figures 8 and 9 show a sample set of ring−disk measurements with the alloy catalysts in comparison with the standard Pt catalyst in O_2-saturated 0.1 M $HClO_4$ at 60 °C. Following a potential region where the ORR is under mixed kinetic-diffusion control, well-defined diffusion limiting currents were recorded in the potential range between 0.1 to about 0.6 V. The ring currents amount to negligible fractions of the disk currents in the potential region above 0.6 V, which indicates that the ORR proceeds without production of peroxide in solution throughout the potential region for oxygen reduction. A slight decrease in the disk currents with a concurrent increase in the ring currents can be observed in the H_{upd} potential region. This is a clear indication of enhanced peroxide production on both the Pt and the alloy catalysts in the H_{upd} region. Qualitatively similar results were reported previously for Pt single-crystal electrodes, and the full discussion of the change in the ORR pathway in this potential region is presented there.[25] Presumably the same reaction mechanism applies to these supported Pt-rich nanoparticles; i.e., H_{upd} blocks the Pt ensembles needed to break the O−O bond leading to peroxide production.

The PtNi catalyst produced significantly different results (not shown). The ring and disk current curves look qualitatively similar but are shifted in potential. The disk currents are shifted to a lower potential, e.g., about 60 mV at 3 mA/cm^2, in comparison to the other supported catalysts. The peroxide production increases continuously starting from potentials below 0.7 V, reaches a kind of plateau between 150 and 300 mV, and increases rapidly for potentials below 0.2 V. At 0.4 V at room temperature, the peroxide yield from PtNi is more than twice that from Pt or Pt_3Ni. However, as we noted in the previous section, the behavior of this catalyst is quite unstable in the ORR potential region, especially at 60 °C. For that reason we have not shown the curves in a figure, nor have we attempted to analyze the results in any detail.

The inset D in Figures 8 and 9 presents a plot of i^{-1} vs $\omega^{-0.5}$ for various potentials obtained on the 75% Pt alloy catalysts at room temperature. Essentially identical plots were obtained with the standard Pt catalyst. The slope of the lines, the so-called *B* factor, allows us to check the for consistency with the theoretical

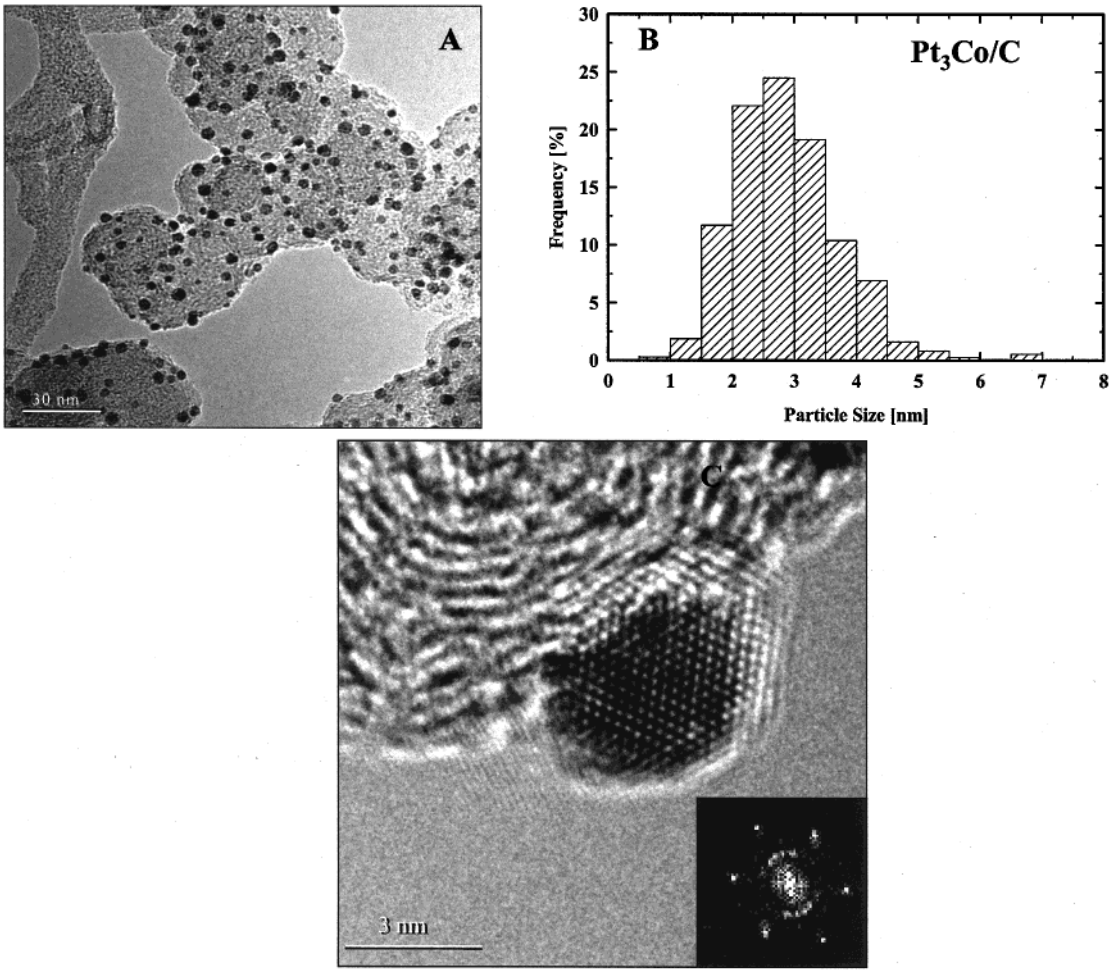

Figure 4. (a) Low-magnification HREM micrograph. (b) Particle size distribution determined by HREM micrographs. (c) HREM micrograph with atomic resolution of the Pt-25 at. % Co (Pt_3Co) catalyst.

TABLE 3: Comparison of Tafel Slopes and Enthalpies of Activation Determined on Pt/Vulcan and the Alloy Catalyst

catalyst	Tafel slope @ 20 °C (mV/dec) lcd/hcd[a]	Tafel slope 60 °C (mV/dec) lcd/hcd[a]	ΔH/kJmol^{-1} @ η = 0.30/0.35/0.40 V
Pt/Vulcan	59/107	52/92	21/20/23
Pt_3Ni/Vulcan	51/86	38/75	24/22/26
PtCo/Vulcan	59/73	46/67	24/28/24
Pt_3Co/Vulcan	51/80	45/70	25/28/26

[a] lcd, low current density region; hcd, high current density region.

values according to the relation[19]

$$\frac{1}{i} = \frac{1}{i_k} + \frac{1}{i_f} + \frac{1}{i_d} = \frac{1}{i_k} + \frac{L}{nFC_fD_f} + \frac{1}{BC_0\omega^{1/2}} \qquad (3)$$

where i_k is the kinetic current density, i_f is the diffusion limiting current density in the Nafion film covering the catalyst layer, C_fD_f is the O_2 solubility-diffusivity product in the film, L is the film thickness, and i_d is the diffusion limiting current density through the solution boundary layer. The other terms have their usual meaning. We find $BC_0 = (14.44 \pm 3\%) \times 10^{-2}$ mA cm^{-2} rpm$^{-0.5}$, a value that agrees well with the calculated value of 14.28×10^{-2} mA cm^{-2} rpm$^{-0.5}$ for a four electron ($n = 4$) process using literature data for O_2-solubility (1.18 mol/m^3) [26] and O_2 diffusivity (1.9×10^{-9} m^2 s^{-1}) in low concentrated electrolytic solutions[26] and the viscosity of water (0.893×10^{-2} cm^2 s^{-1}).[27] As expected for Nafion film covered electrodes, the intercept, even at potentials clearly in the so-called limiting current plateau, are not truly zero. This is due to finite values of the film diffusion resistance, $1/i_f$, in eq 3. Using the values of C_fD_f for Nafion-covered Pt solid electrodes,[28] from the intercepts we estimate the Nafion film thickness to be about 0.1 μ (in good agreement with the physical measurement made with a profilometer). However, the film resistance is sufficiently small, e.g., typically 0.01 mA^{-1} cm^2, that for most of the polarization curve the kinetic currents can be obtained from the simpler relation

$$\frac{1}{i} = \frac{1}{i_k} + \frac{1}{i_d} \qquad (4)$$

The inset C in Figures 8 and 9 compares the Tafel plots for the mass transport corrected mass specific current densities (obtained via eq 4) at a rotation rate of 1600 rpm for Pt and the Pt−Ni(Co) alloy catalysts. In addition to having unstable behavior as a cathode material, the PtNi catalyst also exhibited initial performance that was substantially lower than either the Pt standard or Pt_3Ni. Therefore, more detailed analysis of the ORR kinetics was done only on the Pt_3Ni catalyst and the two Pt−Co catalysts.

3.2.3. Kinetic Analysis of the ORR. Figures 8C and 9C show the Tafel plots of the kinetic current densities (per unit geometric area) obtained on Pt and the different alloy catalysts at room temperature and 1600 rpm in the anodic sweep direction (also the data are not shown, the qualitative trend for the current densities obtained at 60 °C is identical). First of all we note that the activity of pure Pt and the alloy catalyst are nearly identical with respect at an identical (total) metal loading. It is

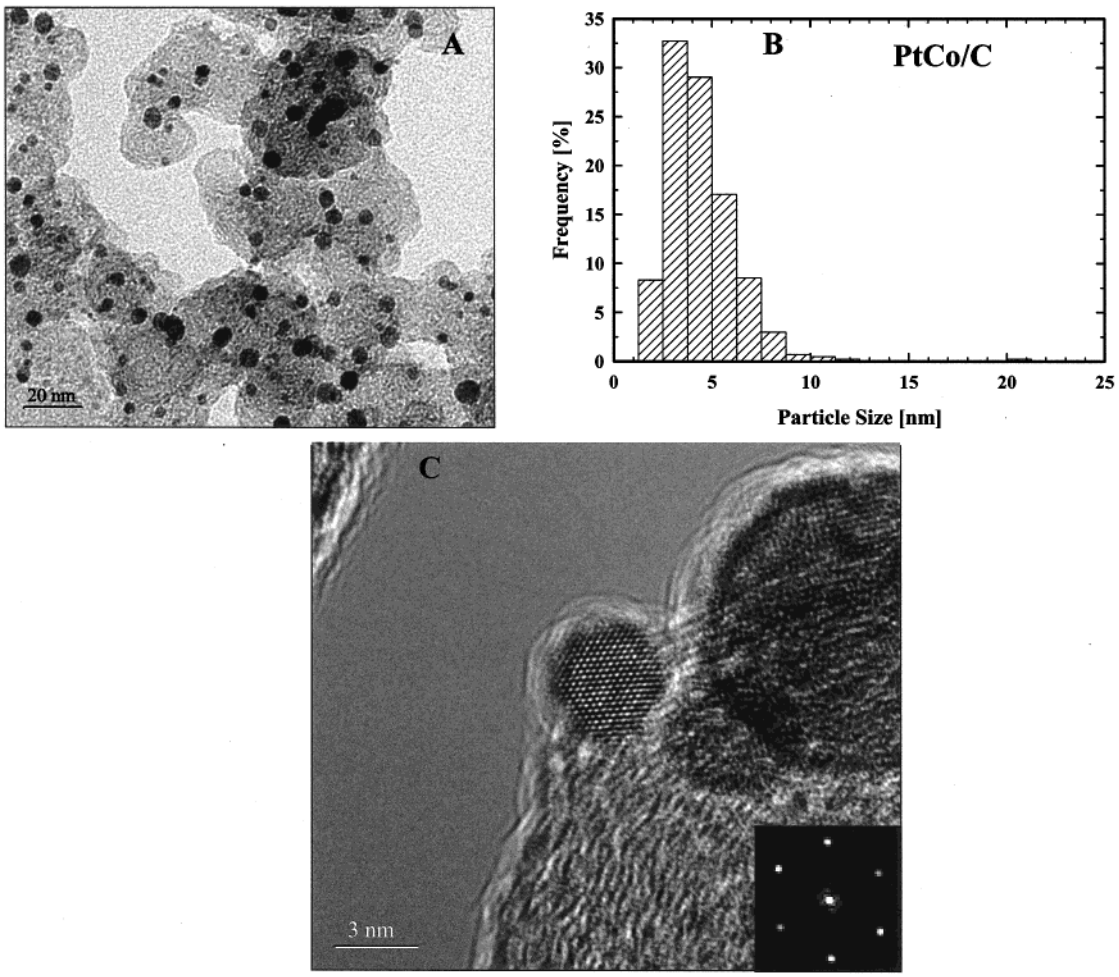

Figure 5. (a) Low-magnification HREM micrograph. (b) Particle size distribution determined by HREM micrographs. (c) HREM micrograph with atomic resolution of the Pt-50 at. % Co (PtCo) catalyst.

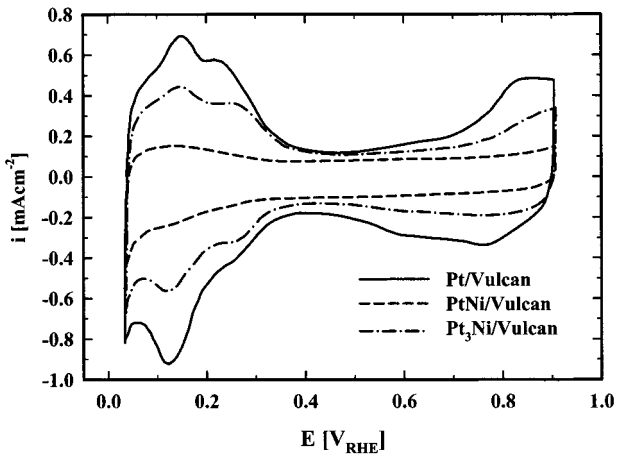

Figure 6. Base voltammograms of the standard supported Pt catalyst compared to the supported Pt_3Ni and PtNi catalyst in argon saturated 0.1 M $HClO_4$ at room temperature, 900 rpm, 50 mV/s; current densities normalized to the geometric electrode area.

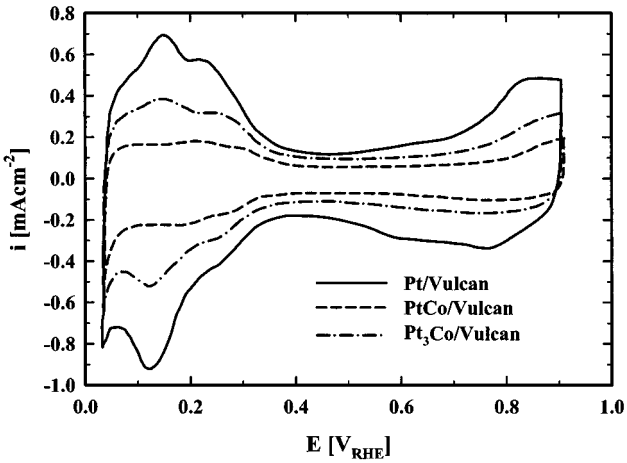

Figure 7. Base voltammograms of the standard supported Pt catalyst compared to the supported Pt_3Co and PtCo catalyst in argon saturated 0.1 M $HClO_4$ at room temperature, 900 rpm, 50 mV/s; current densities normalized to the geometric electrode area.

evident that the Tafel slope changes continuously in the examined potential range, as noted in previous studies of supported Pt catalyst.[25,29] We nevertheless fitted the experimental data to two Tafel slope regions at low and high overpotential to enable a comparison with the literature data for solid electrodes. The resulting Tafel slopes at two different temperatures are listed in Table 3. The Tafel slopes for the standard Pt catalyst in 0.1 M $HClO_4$ are lower compared to values reported for single-crystal Pt electrodes,[30] or previously reported values for carbon-supported Pt[18] in 0.05 M H_2SO_4, where ca. $-2.3RT/F$ were obtained at low overpotentials ($E > 0.85$ V) and ca. $-2 \cdot 2.3RT/F$ at high overpotentials ($E < 0.8$ V). Some of this difference can be attributed to the different supporting electrolyte. Comparing single-crystal data obtained in 0.05 M H_2SO_4 to that in 0.1 M $HClO_4$,[25] we find the same qualitative differences in Tafel slopes (lower slopes in 0.1 M $HClO_4$),

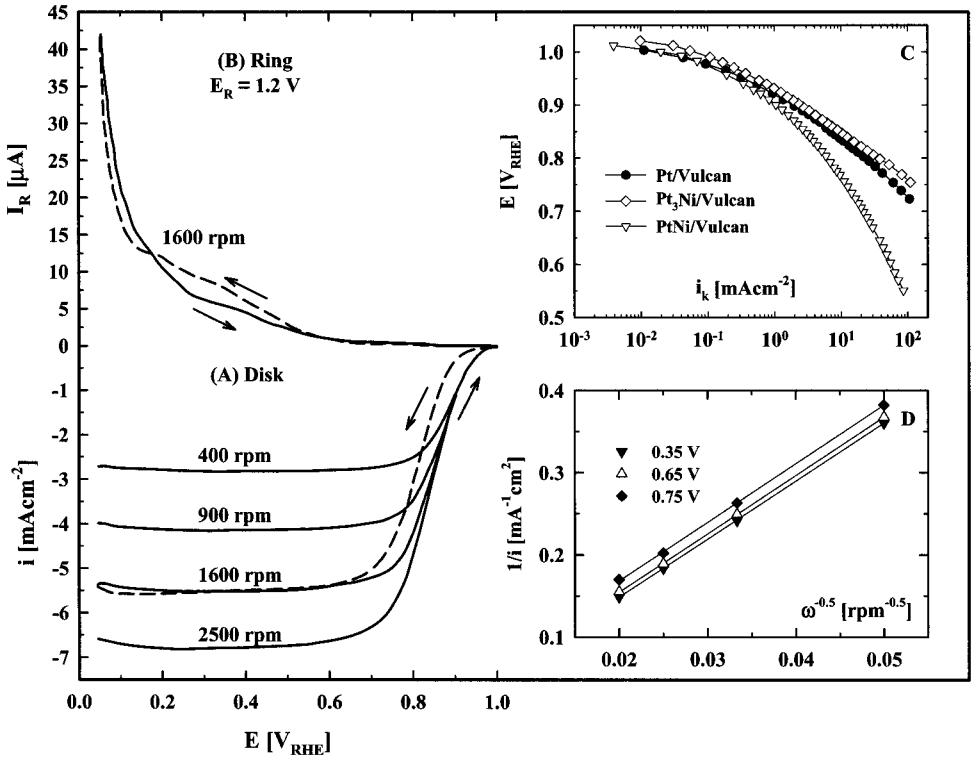

Figure 8. Disk (A) and ring (B) currents obtained during the orr in the anodic sweep (solid lines) and cathodic sweep (dashed lines) on the Pt_3Ni catalyst at room temperature, 5 mV/s. (C) Tafel plots for the ORR at room temperature, anodic sweep 5 mV/s, 1600 rpm on standard Pt, PtNi, and Pt_3Ni catalyst. (D) Levich−Koutecky Plots for the ORR on Pt_3Ni at various potentials extracted from data in (A); current densities normalized to the geometric electrode area.

especially for the Pt(111) and Pt(100) orientations. Since the HREM results clearly indicate that the Pt nanoparticles used in this study consist mostly of Pt(111) and Pt(100) facets, the Tafel slopes are consistent with the above cited literature data. The lower Tafel slopes observed in 0.1 M $HClO_4$ in comparison to data obtained in H_2SO_4 can be attributed to the influence of anion adsorption.[29]

Figure 10 shows plots of the turnover frequency (TOF) as a function of potential. These plots are derived from the kinetic current densities and using the estimate of Pt atom surface density in Table 2, according to the relation,

$$\mathrm{TOF} = \frac{i_k}{neN_s} \tag{5}$$

TOF is an absolute reaction rate, the number of oxygen molecules A being reduced per unit time and per active surface atom, where i_k is the kinetic current density, n is the number of electrons involved in the reaction ($n = 4$ for potentials higher than 0.7 V), and N_s is the number of active surface atoms (in this case we assume only Pt atoms are active). A real activity enhancement per Pt surface atom of about a factor of 1.5−2 can be observed for both of the 75% Pt catalysts, and nearly a factor of 5 for the PtCo catalyst.

The activation enthalpies (ΔH^*) are evaluated at a fixed overpotential using the Arrhenius equation below and following the procedure described previously,[18]

$$\left.\frac{\partial(\log i_k)}{\partial(1/T)}\right|_\eta = \frac{\Delta H^*}{2.3R} \tag{6}$$

using a temperature range between room temperature and 60 °C. The Arrhenius plots for three different overpotentials (η = 300, 350, and 400 mV) for three different catalysts are shown in Figure 11. The activation enthalpies determined from least-squares regressions are essentially identical for the different catalysts, in the considered potential region, and are in the range between 20 and 25 kJ/mol (see Table 3). These values are in close agreement with values reported for Pt single-crystal electrodes in sulfuric acid of ∼25 kJ/mol,[30] for polycrystalline platinum in perchloric acid at 0.8 V (pH = 1.9)[31] of ∼20 kJ/mol, and for values reported previously for carbon-supported Pt in sulfuric and perchloric acid,[18] 26 and 28 kJ/mol, respectively. An activation energy of 28 kJ/mol was also reported using a Nafion covered Pt microelectrode.[32] However, a significantly larger activation energy of ∼60 kJ/mol was reported by Beattie et al.[33] also using a Nafion-coated Pt microelectrode technique, and by Mukerjee et al.[12] using supported Pt catalysts in conventional fuel cell type electrodes with a Nafion membrane. In the former the authors attributed their higher activation enthalpies compared to Parthasarathy et al.[32] to organic impurities from the Nafion solution used to make the recast film, a suggestion with which we concur. In a previous study from this laboratory[16] using solid electrodes of Pt and Pt_3Ni bulk alloy, we reported activation enthalpies between 20 and 25 kJ/mol for both electrodes in a comparable potential range in perchloric acid.

Assuming that the first electron-transfer step is the rate determining step,

$$\mathrm{Pt(O_2)_{ad}} + \mathrm{e^-} \rightarrow \mathrm{Pt(O_2^-)_{ad}} \tag{7}$$

Markovic et al.[34] derived a rate expression using conventional transition state theory given by

$$i = nFkc_{O_2}(1 - \theta_{ad})x \exp(-\beta FE/RT) \exp(-\gamma r\theta_{ad}/RT) \tag{8}$$

where i is the observed current density, n is the number of

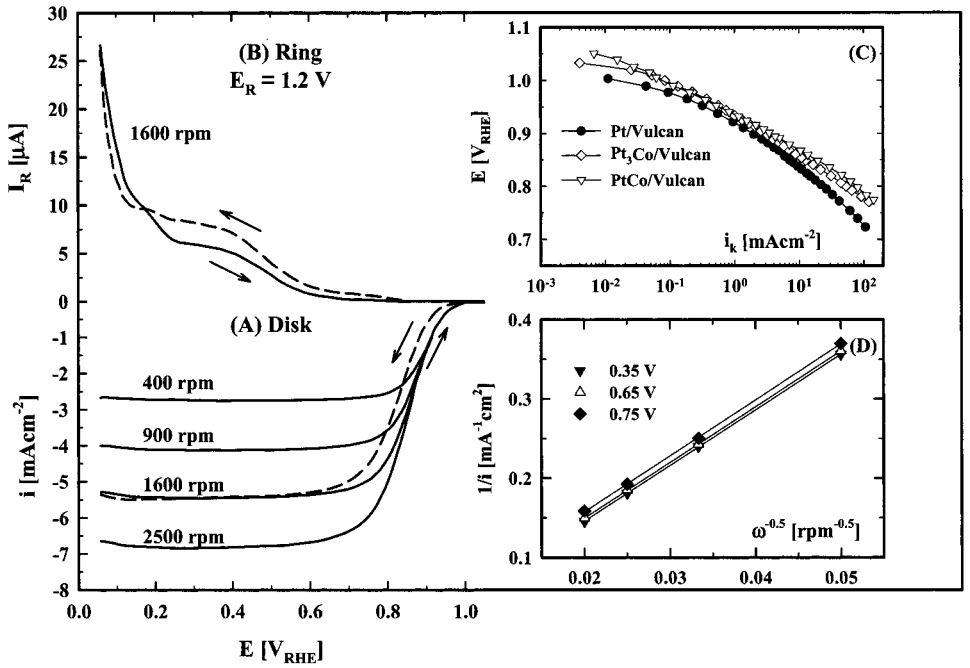

Figure 9. Disk (A) and ring (B) currents obtained during the orr in the anodic sweep (solid lines) and cathodic sweep (dashed lines) on the Pt_3Co catalyst at room temperature, 5 mV/s. (C) Tafel plots for the ORR at room temperature, anodic sweep 5 mV/s, 1600 rpm on standard Pt, PtCo, and Pt_3Co catalyst. (D) Levich−Koutecky Plots for the ORR on Pt_3Co at various potentials extracted from data in (A); current densities normalized to the geometric electrode area.

electrons, k is the (chemical) rate constant, c_{O_2} is the concentration of O_2 in the solution, θ_{ad} is the total surface coverage of adsorbed species (both intermediates and adsorbed anions), E is the applied potential, β and γ are symmetry factors (assumed to be 0.5), and $r\theta_{ad}$ is a parameter characterizing the change in the apparent Gibbs energy of adsorption of oxygeneated species with surface coverage. Note that in general a Tafel plot will be curved, i.e., $(\partial \log i/\partial E)_T$ is a function of potential, only if the $r\theta_{ad}$ term is a *nonlinear* function of potential. The species, which constitute $r\theta_{ad}$ are the intermediates of O_2 reduction and the anions of the supporting electrolyte, which may or may not be adsorbed. Of the possible intermediates only the coverage of OH_{ad} is known independently from cyclic voltammetry, and the adsorption isotherm is available only for some anions mostly on ideal surfaces, like Pt(111). It is reasonable to assume that in perchloric acid we can exclude anion adsorption as an important factor. The potential dependence of OH_{ad} on these supported metallic particles we can see easily in the cyclic voltammetry of Figures 6 and 7. Since the pseudocapacitive current is proportional to the derivative of the coverage of an adsorbed specie,[35,36] we can easily see from the current plateau at $E > 0.8$ V that the coverage by OH_{ad} has a *linear* potential dependence, and thus the Tafel plot should be linear in this potential region, but with a slope that is *not* $2RT/F$ ($\beta = {}^1/_2$). This is the classical result obtained for bulk Pt electrodes (both polycrystal and single crystal) in different electrolytes by many research groups over many years (see review by Adzic[37]). Fundamentally, there is no reason why the Tafel plot for supported Pt should not also be linear in this potential region, unless there are factors unaccounted for in the rate expression given above. At present, we do not know what these factors are. In the potential region below ≈0.8 V, the Tafel plot should show a transition to another linear region where Langmuirian conditions of adsorption apply; i.e., the $r\theta_{ad}$ term is zero and the slope is $2RT/F$ ($\beta = {}^1/_2$). The observation of this transition is more controversial even with solid electrodes, and with supported Pt the reaction rates (TOFs) are so high that it is unlikely one can obtain true kinetic currents. So curved Tafel plots at potentials below ≈0.8 V cannot be considered unexpected. Further examination of the voltammetry in Figures 7 and 8 and the reaction rate theory we have just discussed provide a rationale for the slightly higher activity of the alloy catalysts. As we have seen, both the activation enthalpy and the Tafel slope are essentially identical for the pure Pt and the alloy catalysts, which means that the (chemical) rate constants K and the exponential terms are essentially identical, and the difference must lie in the coverage dependent part of the preexponential term of equation 8, $(1 - \theta_{ad})$. In perchloric acid electrolyte, this term is primarily the OH_{ad} coverage, and as we see from the voltammetry in Figures 6 and 7, the potential region for OH_{ad} is shifted positively by about 50 mV on the alloys versus pure Pt. Qualitatively, this would cause the $(1 - \theta_{ad})$ term to be somewhat larger for the alloy catalysts than for pure Pt, and the factor of 1.5−2 is consistent with the shift of ca. 50 mV in the oxidation potential. It should also be noted that unless θ_{ad} for pure Pt is very close to 1, which occurs only at potentials above ca. 0.95 V, the maximum effect one could see from this term is about a factor of 2−5, not an order of magnitude.

An alternative and/or additional factor to the preexponential term of eq 8 contributing to the difference in kinetics could be the activation entropy, i.e., the configurational entropy of formation of $(O_2^-)_{ad}$. There are no other contributions to the kinetics that we believe would satisfy the observed parameters. It is not clear why Ni or Co in the Pt surface would cause either the shift of ca. 50 mV in the oxidation potential of the Pt surface atoms, and/or change the configurational entropy of formation of $(O_2^-)_{ad}$. We offer here a speculation, not more than that, on why Ni or Co in the Pt surface might cause an anodic shift in the oxidation potential of the Pt surface atoms. If the Ni(Co) atoms are stable in the surface under ORR conditions, they are probably "oxidized" and have one or more OH ligands attached throughout the ORR potential region. These OH ligands could give rise to an effect on OH formation on neighboring Pt atoms analogous to the "common-ion" effect in solution chemistry;[38]

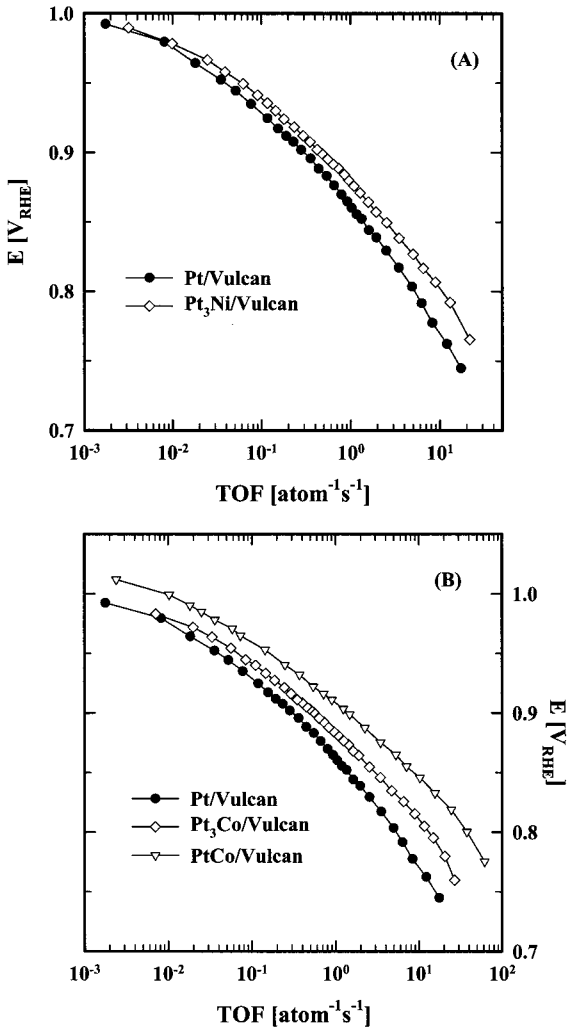

Figure 10. Turn over frequencies (TOF) for (A) standard Pt and Pt_3Ni and (B) standard Pt, PtCo and Pt_3Co at 60 °C calculated from the kinetic current densities using eq 3.

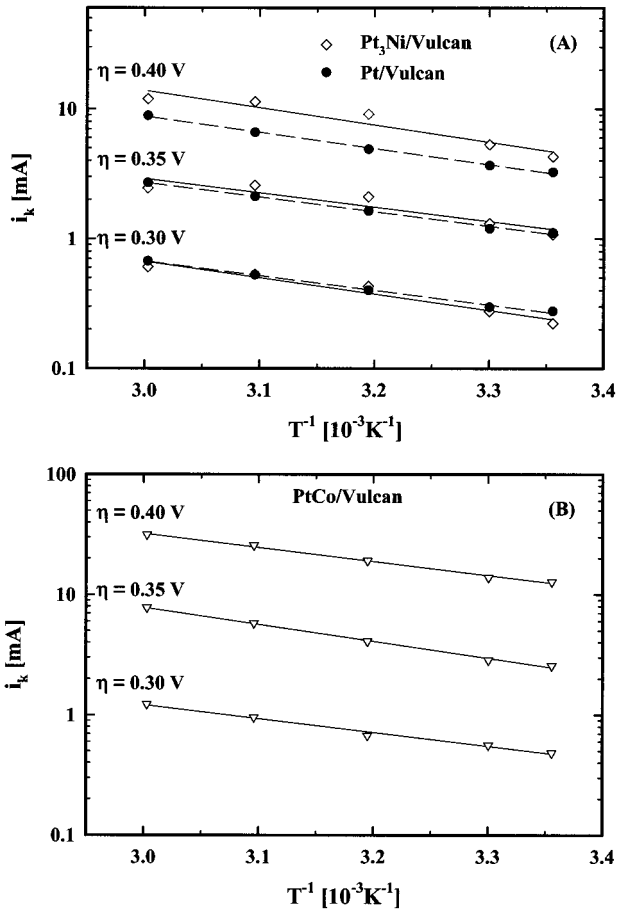

Figure 11. Arrhenius plots for the kinetic current densities for the ORR on (A) standard Pt and Pt_3Ni and (B) PtCo obtained from the anodic sweeps (5 mV/s, 1600 rpm) at different overpotentials in the temperature range between room temperature and 60 °C.

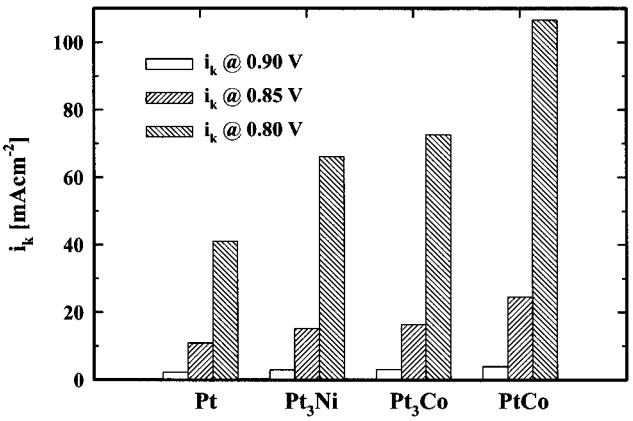

Figure 12. Histogram showing the kinetic current densities at different potentials (geometric current densities) for the catalysts in this study obtained at 60 °C.

i.e., the presence of OH species on the surface repels like species from forming nearby. That explanation would be consistent with the activity per unit Pt surface atom being higher for the PtCo catalyst versus the 75% Pt surfaces. Why only Ni and Co? Many transition metals might be expected to provide the same function, and this may explain why so many Pt-transition metal alloys are reported to have some beneficial effect. They key to this enhancement is (a) the stability of the transition metal in the surface at ORR conditions and (b) achieving the optimum surface composition.

Finally, we comment briefly on the kinetic enhancement we observe with carbon-supported Pt−Ni and Pt−Co in comparison to those reported by others. We observed a small but statistically significant activity enhancement per geometric area on electrodes with equal overall metal loading, very similar particle size, and a very similar Pt surface atom density. An overview of the obtained kinetic current densities per geometric area is given in Figure 12. The so-called mass activity, activity per unit weight of Pt in the catalyst, is enhanced by factors of about 1.5−3 for the alloy catalysts. Based on the Pt surface atom density, the rate per Pt atom (the TOF) is a factor of 1.5−2 higher for Pt_3Ni(Co) and as much as a factor of 5 for PtCo. We found very similar TOF factors using well-characterized bulk metal electrodes of polycrystalline Pt and polycrystalline Pt_3Ni.[16] The activity enhancements observed in this study are generally smaller than those reported by others but are in qualitative agreement with the factors of 2−5 (mass activity) obtained using very similar catalysts in phosphoric acid,[10] and earlier studies by Mukerjee et al.[11−13] or Tamizhmani et al.[14] in PEM electrolyte. In sharp contrast to these results are studies from Toda et al.[15] on several different Pt−Co, Pt−Ni, and Pt−Fe catalysts where an activity (equivalent to our TOF) enhancement of more than a factor of 10 was observed in comparison to pure Pt (in 0.1 M $HClO_4$ at ambient temperature). We will not attempt to reconcile these differences with our results. We do, however, note that the general level of activity for the "pure Pt" case reported by Toda et al. (Figure 10 in ref 16) is

significantly *lower* than data for polycrystalline Pt at exactly the same conditions reported by Damjanovic and co-workers.[39,40] We also note that the catalysts used by Toda et al. are sputtered alloy films that have subjected to an elaborate pretreatment that intentionally corrodes the transition metal from the surface region leaving a so-called Pt "skin". The physical structure of these catalysts makes comparison using either well-characterized bulk alloy or conventional supported catalysts problematic and possibly misleading.

4. Conclusion

We investigated oxygen reduction kinetics on carbon-supported Pt−Ni and Pt−Co alloy catalysts using the thin film RRDE method in 0.1 M $HClO_4$ applying a temperature range between room temperature and 60 °C. Comparison was made to a pure Pt catalyst on the same carbon support, Vulcan XC-72, having the same metal loading (20 wt %) and nominally the same particle size (4 ± 2 nm). High-resolution electron microscopy was used to determine the size and shape of the particles as well as the particle size distribution on all catalysts. Hydrogen adsorption pseudocapacitance was used to determine the number of Pt surface atoms and to estimate the surface composition of the alloy catalysts. Kinetic analysis in comparison to pure Pt revealed a small activity enhancement (per Pt surface atom) of ca. 1.5 for the 25 at. % Ni and Co catalysts, and a more significant factor of 2−3 for the 50 at. % Co. The 50 at. % Ni catalyst was less active than the Pt standard and unstable at oxygen electrode potentials at 60 °C. Ring-current collection measurements for peroxide indicated no significant differences between the Pt−Co catalysts or the 25 at. % Ni catalyst and pure Pt, while the 50 at. % Ni catalyst had a higher peroxide yield. Together with the observed Tafel slopes and activation enthalpies, it was concluded that the kinetic enhancement is contained in the coverage dependent part of the preexponential factor of eq 8 of the conventional transition state theory rate expression. It is, however, not clear why the alloying with Ni or Co produces this change in the preexponential factor.

Acknowledgment. The participants in this research from the Lawrence Berkeley National Laboratory acknowledge support from the Office of Advanced Automotive Technologies of the U.S. Department of Energy under contract DE-AC03-76SF00098. The operation of the National Center for Electron Microscopy (NCEM) is funded by the Office of Science, Division of Materials Sciences, of the U.S. Department of Energy. U.A.P.'s research stay at the Lawrence Berkeley National Laboratory was partly financially supported by the Paul Scherrer Institut and the Swiss Federal Office of Energy.

References and Notes

(1) Gottesfeld, S.; Zawodzinski, T. A. Polymer Electrolyte Fuel Cells. In *Advances in Electrochemical Science and Engineering*, 1st ed.; Alkire, R. C., Gerischer, H., Kolb, D. M., Tobias, C. W., Eds.; Wiley-VCH: Weinheim, 1997; Vol. 5; p 195.

(2) Wilson, M. S.; Gottesfeld, S. *J. Appl. Electrochem.* **1992**, *22*, 1.

(3) Wilson, M. S.; Valerio, J. A.; Gottesfeld, S. *Electrochim. Acta* **1995**, *40*, 355.

(4) Stonehart, P. *Ber. Bunsen-Ges. Phys. Chem.* **1990**, *94*, 913.

(5) Luczak, F. J.; Landsman, D. A. Ternary Fuel Cell Catalysts Containing Platinum, Cobalt and Chromium. U.S. Patent No. 4447506, 1984.

(6) Luczak, F. J.; Douglas, A. Ordered Ternary Fuel Cell Catalysts Containing Platinum and Cobalt. U.S. Patent No. 4711829, 1987.

(7) Luczak, F. J.; Landsman, D. A. Ordered Ternary Fuel Cell Catalysts Containing Platinum and Cobalt and Method for Making the Catalysts. U.S. Patent No. 4677092, 1987.

(8) Beard, B.; Ross, P. *J. Electrochem. Soc.* **1990**, *137*, 3368.

(9) Glass, J. T.; Cahen, G. L.; Stoner, G. E.; Taylor, E. J. *J. Electrochem. Soc.* **1987**, *134*, 58.

(10) Min, M.; Cho, J.; Cho, K.; Kim, H. *Electrochim. Acta* **2000**, *45*, 4211.

(11) Mukerjee, S.; Srinivasan, S. *J. Electroanal. Chem.* **1993**, *357*, 201.

(12) Mukerjee, S.; Srinivasan, S.; Soriaga, M. P. *J. Phys. Chem.* **1995**, *99*, 4577.

(13) Mukerjee, S.; Srinivasan, S.; Soriaga, M. P.; McBreen, J. *J. Electrochem. Soc.* **1995**, *142*, 1409.

(14) Tamizhmani, G.; Capuano, G. A. *J. Electrochem. Soc.* **1994**, *141*, 968.

(15) Toda, T.; Igarashi, H.; Uchida, H.; Watanabe, M. *J. Electrochem. Soc.* **1999**, *146*, 3750.

(16) Stamenkovic, V.; Schmidt, T. J.; Paulus, U. A.; Radmilovic, V.; Markovic, N. M.; Ross, P. N. *Meeting Abstracts*, ECS Fall Meeting, The Electrochemical Society, Inc., San Francisco, CA., 2001; Abstract No. 1053.

(17) Schmidt, T. J.; Gasteiger, H. A.; Stäb, G. D.; Urban, P. M.; Kolb, D. M.; Behm, R. J. *J. Electrochem. Soc.* **1998**, *145*, 2354.

(18) Paulus, U. A.; Schmidt, T. J.; Gasteiger, H. A.; Behm, R. J. *J. Electroanal. Chem.* **2001**, *495*, 134.

(19) Schmidt, T. J.; Paulus, U. A.; Gasteiger, H. A.; Alonso-Vante, N.; Behm, R. J. *J. Electrochem. Soc.* **2000**, *147*, 2620.

(20) Pearson, W. B. *A Handbook of Lattice Spacings and Structures of Metals and Alloys*; Pergamon Press: London, 1958.

(21) Markovic, N. M.; Gasteiger, H. A.; Ross, P. N., Jr. *Langmuir* **1995**, *11*, 4098.

(22) Denton, J.; Gascoyne, J. M.; Thompsett, D. Materials for use in catalytic electrode manufacture. European Patent No. EP 731520A1, 1996.

(23) Conway, B. E.; Angerstein-Kozlowska, H.; Sharp, W. B. A. *J. Chem. Soc., Faraday Trans.* **1978**, *74*, 1373.

(24) Paulus, U. A.; Schmidt, T. J.; Stamenkovic, V. R.; Markovic, N. M.; Ross, P. N. Oxygen Reduction Activity of Pt and Pt−Alloys in Acid Electrolyte; In *1st European PEFC Forum, Proceedings*, Büchi, F. N., Scherer, G. G., Wokaun, A., Eds.; European Fuel Cell Forum: Oberrohrdorf, 2001; p 51.

(25) Markovic, N.; Gasteiger, H.; Ross, P. N. *J. Electrochem. Soc.* **1997**, *144*, 1591.

(26) Gubbins, K. E.; Walker, R. D., Jr. *J. Electrochem. Soc.* **1965**, *112*, 469.

(27) Weast, R. E. In *CRC Handbook of Chemistry and Physics*, 66 ed.; CRC Press: Boca Raton, Fl., 1986.

(28) Zecevic, S. K.; Wainright, J. S.; Litt, M. H.; Gojkovic, S. L.; Savinell, R. F. *J. Electrochem. Soc.* **1997**, *144*, 2973.

(29) Uribe, F. A.; Springer, T. E.; Gottesfeld, S. *J. Electrochem. Soc.* **1992**, *139*, 765.

(30) Grgur, B. N.; Markovic, N. M.; Ross, P. N. *Can. J. Chem.* **1997**, *75*, 1.

(31) Sepa, D. B.; Vojnovic, M. V.; Vracar, L. M.; Damjanovic, A. *Electrochim. Acta* **1986**, *31*, 91.

(32) Parthasarathy, A.; Srinivasan, S.; Appleby, A. J.; Martin, C. R. *J. Electrochem. Soc.* **1992**, *139*, 2530.

(33) Beattie, P. D.; Basura, V. I.; Holdcroft, S. *J. Electroanal. Chem.* **1999**, *468*, 180.

(34) Markovic, N. M.; Gasteiger, H. A.; Grgur, B. N.; Ross, P. N. *J. Electroanal. Chem.* **1999**, *467*, 157.

(35) Conway, B.; Angerstein-Kozlowska, H. *J. Electroanal. Chem.* **1980**, *113*, 63.

(36) Conway, B.; Angerstein-Kozlowska, H.; Ho, F. *J. Vac. Sci. Technol. A* **1977**, *14*, 351.

(37) Adzic, R. Recent Advances in the Kinetics of Oxygen Reduction. In *Electrocatalysis*; Lipkowski, J., Ross, P. N., Eds.; Wiley-VCH: New York, 1998; p 197.

(38) Conway, B. Ionic Hydration in Chemistry and Biophysics. In *Ionic Hydration in Chemistry and Biophysics*; Elsevier Scientific Publishing: New York and Amsterdam, 1981; p 417.

(39) Paucirova, M.; Drazic, D. M.; Damjanovic, A. *Electrochim. Acta* **1973**, *18*, 945.

(40) Sepa, D. B.; Vojnovic, M. V.; Damjanovic, A. *Electrochim. Acta* **1981**, *26*, 781.